Surface water iron supplies in the Southern Ocean sustained by deep winter mixing

Alessandro Tagliabue[1,2*], Jean-Baptiste Sallée[3,4,5], Andrew R. Bowie[6], Marina Lévy[3,4], Sebastiaan Swart[2,7] and Philip W. Boyd[8,9]

[1]Department of Earth, Ocean and Ecological Sciences, School of Environmental Sciences, University of Liverpool, Liverpool, L69 3GP, United Kingdom.

[2]Southern Ocean Carbon and Climate Observatory, CSIR, Stellenbosch, South Africa

[3]Sorbonne Universités, UPMC Univ., Paris 06, UMR 7159, LOCEAN-IPSL, F-75005, Paris, France

[4]CNRS, UMR 7159, LOCEAN-IPSL, F-75005, Paris, France

[5]British Antarctic Survey, High Cross, Cambridge, CB3 0ET, United Kingdom,

[6]Antarctic Climate and Ecosystems CRC, University of Tasmania, Private Bag 80, Hobart, Tasmania 7001, Australia.

[7]Department of Oceanography, Marine Research Institute, University of Cape Town, Rondebosch, 7701, South Africa

[8]NIWA Centre of Chemical & Physical Oceanography, Department of Chemistry, University of Otago, Dunedin, New Zealand

[9]Institute for Marine and Antarctic Studies, University of Tasmania, Private Bag 129, Hobart, Tasmania 7001, Australia.

[*]Corresponding author: a.tagliabue@liverpool.ac.uk

Iron regulates Southern Ocean primary productivity and due to geographically restricted surface inputs (e.g. local dust supply), most dissolved iron (DFe) is supplied at a basin-scale to surface waters from subsurface reservoirs (remineralisation and sediment/hydrothermal inputs). The main physical processes are deep winter mixing (entrainment) and year-round diffusion across density surfaces (diapycnal diffusion). The relative importance of each

remains observationally poorly constrained, yet ultimately governs the climate sensitivity of regional productivity. Here we show that winter entrainment determines the DFe supply to Southern Ocean phytoplankton to a greater extent than diapycnal diffusion, necessitating a strong seasonal reliance on biologically recycled iron. DFe observations are combined with hydrography from Argo floats and biological utilisation estimates to determine basin-scale, observationally constrained DFe fluxes. Weak vertical gradients reduce the importance of diapycnal diffusion to seasonal re-supply and instead, a 'one off' deep wintertime entrainment pulse annually replenishes surface DFe stocks. Following DFe depletion, biological observations from the sub-Antarctic sector suggest intense upper-ocean DFe recycling that sustains productivity. Accordingly, entrainment and recycling are likely important drivers of temporal variations in Southern Ocean primary production. Our results are underpinned by the nature of vertical DFe gradients, making these features important constraints on ocean models.

The micronutrient iron (Fe) is an important regulator of primary productivity and therefore the strength of the biological carbon pump in the Southern Ocean[1,2]. This region is of key importance to both the global carbon cycle and air-sea carbon dioxide fluxes[3,4] and the impact of future or past climate variability is mediated to a large degree by modifications to Fe supply to the biota[5]. Despite a marked expansion of DFe observations in the 'GEOTRACES' era[6] and several investigations[7,8] into the magnitude of exogenous inputs of dissolved Fe (DFe, $t<0.2\mu m$), little attention has been focussed on the physical processes that supply DFe at the basin-scale from subsurface reservoirs, enriched in DFe from both external inputs[1,8] and remineralisation[9]. In general, wintertime deep mixing (or entrainment), year-round vertical diapycnal diffusion and Ekman upwelling/downwelling are the major physical processes involved in the vertical supply of DFe to phytoplankton[10-12]. The maximum depth of mixing over the year (MLD_{MAX}) and the DFe inventory within this stratum control the degree of DFe entrainment. Diapycnal diffusion depends on the

vertical diffusivity (k_z) and the vertical DFe gradient at the base of the MLD ($\partial Fe/\partial z_{MLD}$), while the Ekman upwelling/downwelling of DFe depends on the wind stress curl and the concentration of DFe at the base of the mixed-layer. In terms of their drivers, entrainment is primarily controlled by air-sea surface buoyancy fluxes, while Ekman upwelling/downwelling responds to momentum forcing from winds, and near-surface diapycnal diffusion extracts its energy from a range of sources including winds and buoyancy. As each of these factors will be differentially altered by climate change[5,13], understanding the climate sensitivity of vertical DFe supply to Southern Ocean phytoplankton depends upon the relative role played by different physical input pathways. Despite prior attempts[10,11], the importance of each physical pathway is poorly quantified due to historically-sparse data coverage and this shortcoming hampers efforts to constrain the response of Southern Ocean biogeochemical cycling to climate change.

A key influence on the vertical input of DFe to the mixed-layer is exerted by its water column profile and in particular, the location and magnitude of vertical concentration gradients ($\partial Fe/\partial z$). The depth at which $\partial Fe/\partial z$ is maximal is termed the 'ferricline' (hereafter: $Z_{Fe,}$ supplementary figure 1), and as for nitrate (and the 'nitracline'), is critical in understanding how changes in winds and buoyancy fluxes will impact physical DFe supply processes. Like nitrate stocks in the North Atlantic, DFe concentrations are typically depleted (not necessarily to zero) in Southern Ocean surface waters during spring/summer[6] due to biological consumption and prevailing DFe limitation[14], with greater subsurface concentrations from organic matter remineralisation. However, unlike nitrate, Fe is also lost from the dissolved pool due to particle scavenging, has important subsurface inputs from ocean sediments and hydrothermal vents[1,8] and is likely remineralised more slowly[15,16], such that Z_{Fe} can be deeper than both the nitracline and MLD[15,17-19]. However, the nature of the depth offset between Z_{Fe} and MLD across the wider Fe-limited Southern Ocean and its relation to physical DFe supply processes remains uncertain. If Z_{Fe} were to be consistently deeper than the MLD at basin scales, this would have important implications for the magnitude of vertical

DFe supply and its seasonal variability, highlighting the unique nature of Fe cycling. Here we use a novel approach that synthesises recent DFe observations (including recent GEOTRACES field campaigns)[6], co-localised MLDs from the Argo float archive[20] and satellite phytoplankton Fe utilisation estimates[7] (see Methods) to quantify the processes responsible for the seasonal supply of DFe in the Southern Ocean for the first time. Our goals were to document Z_{Fe} depths, their relation to MLDs and to quantify the spatial variability in the supply of DFe from entrainment, diapycnal mixing and Ekman upwelling/downwelling across the Southern Ocean.

Ferricline Depth and Quantifying Vertical Iron Supply

Due to its fundamental role in regulating DFe inputs, we first determined Z_{Fe} across the Southern Ocean. The mean depth of Z_{Fe} was 333m (median of 350m) across the 140 unique determinations (Figure 1a). Much of the variability in Z_{Fe} in absolute depth is eliminated when the potential density anomaly (σ_θ, kg m^{-3}; referenced at the ocean surface) at the depth of Z_{Fe} is plotted (determined from Argo profiling floats; Figure 1b). Consistent across all sampled Southern Ocean sectors, we find that Z_{Fe} is typically associated with denser waters south of the Polar Front ($\sigma_\theta >$ 27.5 kg m^{-3}) and with lighter waters ($\sigma_\theta <$ 27.5 kg m^{-3}) further north, with a striking decline in σ_θ at Z_{Fe} from south to north (Figure 1b). Since σ_θ declines at any depth from south to north, modifications to isopycnal depths likely drive a large part of the variability in the absolute depth of Z_{Fe} (Figure 1, especially at relatively adjacent locations) probably following some 'preconditioning' from Fe-specific biogeochemical processes (encapsulated by longer remineralisation length scales[15]). The vertical gradient at Z_{Fe} ($\partial Fe/\partial z_{ZFe}$) is generally much greater than that at the MLD ($\partial Fe/\partial z_{MLD}$), which indicates that Z_{Fe} is the most significant vertical gradient in the upper 1000m (Supplementary Figure 2). Moreover, $\partial Fe/\partial z_{ZFe}$ is greatest (meaning a 'sharper' ferricline) in the south Atlantic sector, illustrating the signature of DFe subsurface lateral transfer from numerous regional islands[1,7] in the DFe profiles. On average, Z_{Fe} is deeper than the co-located MLD by 245m

(median = 210m, Figure 2a), with no seasonal bias where data are available (Figure 1c). As a measure of MLD variability, the offset changes to 199m or 288m using MLDs at +2σ or -2σ, respectively (see methods for details on the computation of the standard deviation, σ). Thus irrespective of the time of year, we demonstrate that Z_{Fe} is robustly and significantly deeper than the MLD across much of the Southern Ocean. That nitracline and phosphocline depths are more closely coupled to the MLD illustrates unique behaviour of DFe in this regard (Supplementary Figure 3).

That Z_{Fe} is almost always much deeper than the concomitant MLD indicates limited input of DFe from diapycnal diffusion due to weak $\partial Fe/\partial z_{MLD}$ (supplementary Figure 2b). For example, applying typical Southern Ocean k_z values[18,21-23] of 10^{-5} to 10^{-4} m^2 s^{-1} results in 1.6-15.7 nmol DFe m^{-2} d^{-1} from diapycnal diffusion input. Across all combinations of MLD and k_z (i.e. ±2σ for MLD and 10^{-5}-10^{-4} for k_z), diapycnal diffusion is 0.25-7.7 μmol DFe m^{-2} yr^{-1} (Figure 2b; consistent with estimates from occasional *in situ* studies[14,16,17,24]). The highest rates of diapycnal diffusion DFe input are found near the Antarctic Peninsula and are comparable to recent regional observations[24]. However such values do not appear generally representative of the offshore Southern Ocean, where diapycnal diffusion inputs of <0.2 μmol DFe m^{-2} yr^{-1} generally prevail (Figure 2b).

In contrast to diapycnal diffusion, the winter entrainment pulse can supply much more DFe. Entrainment is quantified using winter mixed-layer depths (MLD_{MAX}) from ARGO profiles, alongside estimated winter Z_{Fe} (Z_{FeMAX}, see methods). While winter mixing depths exceed Z_{FeMAX} more often, the mean offset remains 212m (median = 143m, Figure 2a), similar to the sole winter DFe section[25]. At ±2σ on MLD_{MAX}, mean offsets are 114m and 311m. To correctly compute net entrainment inputs also requires a consideration of the DFe stocks that are detrained during springtime mixed-layer shallowing, which can be estimated using Argo profiling data at each DFe profile location. Ultimately, the mean entrainment Fe input is 21.1 μmol DFe m^{-2} yr^{-1}, or 9.5-33.2 μmol DFe m^{-2} yr^{-1} at ±2σ on MLD_{MAX}. This is more than 10-fold greater (on average) than the

131 annual diapycnal diffusion inputs estimated above. Spatially (Figure 2c), entrainment inputs are
132 higher than average around the Antarctic Peninsula and some parts of the Indian and Pacific sectors
133 of the Southern Ocean. Much lower entrainment fluxes are present in many other regions due to
134 weak vertical gradients in DFe persisting down to MLD_{MAX}. That appreciable entrainment fluxes
135 DFe arise despite ~200m offsets persisting between Z_{FeMAX} and MLD_{MAX} highlights the smaller
136 vertical gradients in DFe at the top of the ferricline (but shallower than Z_{FeMAX}) that are captured by
137 winter mixing.
138
139 Ekman upwelling and downwelling is computed using DFe concentrations at the mixed-layer base
140 and the wind stress curl (Figure 2d). Ekman fluxes are strongly latitude-dependent, switching from
141 net losses to gains of DFe as the sign of the wind stress curl changes across the atmospheric
142 subtropical jet (Figure 2d). In general, Ekman fluxes are comparable to those associated with
143 diapycnal diffusion, rather than entrainment, and on average are a slight net loss of DFe from the
144 system (-0.7 μmol DFe m^{-2} yr^{-1} or a median of -0.4 μmol DFe m^{-2} yr^{-1}), although this is likely
145 sensitive to the sampling frequency north and south of the atmospheric subtropical jet. Finally,
146 transient MLD deepening during the phytoplankton growth season might entrain additional Fe, but
147 using the rate of change in the MLD from Argo floats 10 days either side of the sampling date, we
148 found this process to be negligible.
149
150 Additional regional or localised sources of DFe to the mixed layer are provided from dust
151 deposition[26] and melting of sea ice[27] or icebergs[28,29] and glaciers[29,30]. Estimates of their supply rates
152 are difficult to generalise as they are usually derived from models or point-source observations that
153 are not easily extrapolated to basin scales. Upper limits[7] for dust deposition, sea ice melting and
154 icebergs are on the order of 20 μmol DFe m^{-2} yr^{-1}, making them comparable to entrainment.
155 However, it is notable that many of these additional DFe fluxes are extremely localised[7] and these
156 upper limits will only be realised close to sources (i.e. nearshore waters). Therefore over much of

157 the offshore Southern Ocean that is the focus of this study, their contribution to DFe supply will be
158 greatly reduced. The major basin-scale role we find for entrainment is similar to a recent study
159 conducted at one station in the, oceanographically very different, western North Pacific[31].
160
161 **Iron Supply and Utilisation**
162
163 We now consider how diapycnal diffusion and entrainment DFe sources can meet estimates of
164 biological Fe utilisation. Basin-scale quantifications of phytoplankton Fe utilisation rely on
165 combining estimates of net primary production with algal Fe utilisation from laboratory culture
166 experiments[7]. Direct comparison with our physical input terms is complicated as much of the Fe
167 utilisation is met from recycled Fe, illustrated by *f*e-ratios (proportion of Fe uptake from 'new'
168 sources[17]) that range between 0.06 and 0.5 from low to high DFe waters[14,16,17,32]. Moreover,
169 phytoplankton only represent about half of total Fe utilisation associated with microbial and
170 metazoan assemblages[1]. Lastly, the quantification of diapycnal diffusion and entrainment are
171 sensitive to assumptions regarding k_z and (to a lesser extent) the degree of detrainment,
172 respectively. Nevertheless, by exploring the plausible parameter space for the *f*e-ratio, k_z and
173 detrainment we can assess the capacity for diapycnal diffusion and entrainment to meet
174 phytoplankton Fe utilisation (where DFe data are presently available). When k_z is low, diapycnal
175 diffusion cannot match utilisation in >50% of locations, regardless of *f*e-ratios (Figure 3a). Even
176 when k_z approaches its upper limit of 10^{-4} m^2 s^{-1}, diapycnal diffusion meets utilisation in >50% of
177 cases only when the *f*e-ratio reaches unrealistically low levels (i.e., minimal reliance on new Fe,
178 Figure 3a). In contrast, it is only when the detrainment term is greatest (~3-fold higher than the
179 Argo float data average of 3.1) and the *f*e-ratio is maximal (i.e. greatest reliance on new Fe) that
180 entrainment cannot meet utilisation in >50% of cases (Figure 3b). As more DFe data are collected
181 in the offshore Southern Ocean then the importance of diapycnal diffusion would likely further
182 decline. When examined spatially, even in locations where diapycnal diffusion is strong (e.g. near

183 the Antarctic Peninsula, Figure 2b), it only provides ~10-20% of total DFe inputs from physically-
184 mediated fluxes (Figure 3c). In contrast, entrainment always provides >60% of total DFe input
185 (Figure 3d) and is often able to offset regional losses of DFe due to Ekman downwelling (Figure
186 2d). Thus it seems diapycnal diffusion is rarely a significant component of seasonal DFe supply in
187 the Southern Ocean, which we suggest is dominated by a 'one-off' pulse of new DFe via winter
188 entrainment. It is noteworthy in this context that entrainment can always match available estimates
189 of iron utilisation (supplementary material).
190
191 Our results permit an illustration of the key processes involved in the supply and cycling of DFe
192 over the Southern Ocean phytoplankton growth season (Figure 4). Deep winter mixing maximises
193 access to subsurface DFe reservoirs and re-stocks the mixed-layer. During spring, this inventory is
194 depleted rapidly (days to weeks) by both the upper ocean biota[14] and abiotic scavenging onto
195 settling particles. Diapycnal diffusion will therefore become the major DFe supply term from late
196 spring onwards, but its low rates (~7-21 nmol DFe m^{-2} d^{-1}) cannot be reconciled with measured
197 mixed-layer phytoplankton utilisation[14,16,17,32,33] of ~2-6 μmol DFe m^{-2} d^{-1}. Phytoplankton are
198 therefore heavily reliant on DFe from pelagic recycling, with *f*e-ratios declining accordingly over
199 summer[14]. This highlights the importance of the 'ferrous wheel'[33] in late spring and summer when
200 DFe inputs to the mixed-layer are weak. Indeed, measured Fe regeneration rates of 5-10 μmol m^{-2} d^{-1}
201 more closely match phytoplankton requirements[14]. We suggest that an increasing importance of
202 recycled Fe due to low diapycnal diffusion inputs would cause a shift from initially high *f*e-ratios to
203 lower *f*e-ratios over the year. This may prove disadvantageous to larger phytoplankton such as
204 diatoms and favour smaller phytoplankton cells[14]. The relative magnitudes of winter DFe
205 replenishment of the mixed-layer by entrainment and on-going diapycnal diffusion is mediated by
206 the degree of coupling between Z_{Fe} and the MLD over the year (e.g. Figures 1c, 2a). However, due
207 to the persistent offsets between Z_{Fe} and the MLD (Figure 2a), winter entrainment dominates DFe
208 supply over much of the Southern Ocean (Figure 3d), with little vertical DFe input to the biota from

spring onwards (Figure 4). This emphasises the role of Fe recycling by herbivory, bacterivory and virally-mediated microbial mortality in regulating the mixed-layer DFe pool until the mixed-layer deepens again in autumn. Accordingly, better understanding the dynamics of DFe turnover rates and the associated bioavailability of recycled DFe would be an important future focus.

Our conceptual model posits that because Z_{Fe} is so deep, recycling is crucial in maintaining mixed-layer DFe stocks following the pulse of DFe from entrainment (Figure 4). The detailed biological rate data supporting this view has been obtained from detailed process studies conducted in the Sub Antarctic Zone of the Southern Ocean[15-17,32,33]. Turning to the silicate-rich waters of the Antarctic Zone, our analysis suggests that the paradigm of significant winter entrainment input of DFe followed by little subsequent 'irrigation' from diapycnal iron supply is also true (Figure 3c d). But in addition to Fe recycling, it is also plausible that additional biological factors might influence the seasonal cycle of biological productivity south of the Polar Front in the Antarctic Zone. For example, heavily-silicified diatoms are more common here and their 'luxury uptake' of DFe[34,35] early in the spring (when mixed layer DFe stocks remain high) may help sustain diatom cell division once this wintertime DFe pulse has been depleted. Nevertheless, any region-specific additional processes, such as luxury uptake of iron, would only serve to complement recycling as a key determinant of phytoplankton growth once the influence of entrained iron ceases in spring/summer (Figure 4).

Implications for Southern Ocean Carbon Cycling

DFe regulates phytoplankton growth throughout the Southern Ocean[1,2], hence basin-scale fluctuations in Southern Ocean primary productivity[36] should be linked to changing DFe inputs. Our initial results would suggest an important role for entrainment, as mediated by winter mixing in this context (Figure 3d). Indeed, using a scale analysis we find inter-annual variation in DFe supply

235 from entrainment is 9.1-33 μmol m^{-2} yr^{-1}, as compared to 1.2-3.6 or -1.9-0.4 μmol m^{-2} yr^{-1} from
236 diapycnal diffusion or Ekman, respectively. Inter-annual modifications to dust deposition[37,38], or the
237 melting of sea ice[39] might also be important locally (perhaps ranging 2 to 8 fold[7]), but these inputs
238 cannot readily be extrapolated to basin scales. Inter-annual basin-scale changes in Southern Ocean
239 primary production presently can only be assessed by satellite and are estimated[36] at ~ ±11% (from
240 1997-2006). This variability is relatively small in contrast to the large changes in wintertime DFe
241 inputs we estimate and the widely demonstrated role DFe supply plays in setting regional
242 productivity[2]. Robust attribution of causality to the driver(s) of observed fluctuations in remotely-
243 sensed basin-scale primary productivity is so far lacking for the Southern Ocean[36]. Such attribution
244 may be further masked by the unique bio-optical properties of Southern Ocean waters that likely
245 hinder the utility of remotely-sensed productivity datasets[40]. Satellite estimates may be further
246 confounded by the complicated inter-play between physical DFe supply, external DFe inputs and
247 physiological plasticity in phytoplankton DFe utilisation[7]. Nevertheless, our results show winter
248 entrainment is pivotal to regional DFe supply and must be part of a future appraisal of the
249 sensitivity of Southern Ocean productivity to basin-scale environmental fluctuations, which has
250 been overlooked in previous assessments[36,41].
251
252 Properly accounting for the role of winter entrainment DFe inputs requires the parallel
253 consideration of winter mixing depths and their connection to subsurface DFe reservoirs (Figure
254 2a). An improved understanding of the distribution of ferricline depths across the Southern Ocean,
255 as part of the GEOTRACES programme, and how they change on seasonal scales would permit a
256 more widespread identification of regions where entrainment dominates. This would, in turn,
257 highlight locations where primary productivity might be more sensitive to variability in buoyancy
258 fluxes rather than winds. In addition, appraising the sensitivity of Fe recycling to environmental
259 factors on seasonal scales is also crucial since it is clearly the major resupply process over spring-
260 summer once entrainment ceases, with probable implications for ecosystem structure (Figure 4).

Finally, climate models seeking to represent the evolution of the Southern Ocean carbon cycle or productivity[42-46] must pay careful attention to their representation of vertical distributions of DFe. The degree of coupling between Z_{Fe} and the MLD in the model will dictate the relative role played by different physical DFe supply mechanisms, as well as the importance of mixed-layer recycling of Fe in sustaining productivity over seasonal and inter-annual periods.

Methods Summary

A global DFe database[6] was re-gridded into 1° x 1° longitude and latitude bins (south of 40°S) by month of sampling and on a depth axis with a 25m resolution in the upper 1000m. The compiled Fe profiles were scrutinised in a number of ways. We firstly required there to be at least one observation shallower than 50m, one observation deeper than 500m and at least five observations in total per profile. The remaining profiles were then interpolated on the vertical axis (see supplementary material) to determine Z_{Fe}. We decided on the most objective definition possible for Z_{Fe}, i.e., the depth at which the $\partial Fe/\partial z$ gradient was maximal (see also:[18]), which avoided assigning a subjective threshold concentration. Alternative methods might be imagined that would allow the capturing of the 'top' and 'bottom' of the ferricline using deviations in $\partial Fe/\partial z$ from zero (Supplementary Figure 1), however they are not easily applied with confidence to such a large dataset. As such our work identifies the 'core' of the ferricline. To avoid deep ocean gradients associated with point sources (e.g., hydrothermal vents) being misidentified as the upper ocean ferricline we restricted our analysis to the upper 1000m where hydrothermal tracers show minimal gradients[8]. Finally, since in coastal systems Z_{Fe} might be very close to the seabed due to sediment input, we decided to remove data where Z_{Fe} was more than 80% of the bottom depth. The total number of unique determinations was 140 or by month: 25 in January, 18 in February, 14 in March, 46 in April, 10 in July, 2 in October, 20 in November and 5 in December. The DFe dataset used in this study is archived and updated here: http://pcwww.liv.ac.uk/~atagliab/LIV_WEB/Data.html.

We calculated the MLD for every Southern Ocean profile with a surface-density difference criterion of $\Delta\sigma_\theta \leq 0.03$ kg m^{-3} [47,48] (Supplementary Figure 1d). The correspondence between Z_{Fe} and MLD was then examined by co-locating MLDs from either in situ CTD profiles and/or Argo profiles[20] (Supplementary Figure 2d) for the same month and year within 2.5 degrees of a Z_{Fe} determination and weighted by $1/d^4$ (where d is the distance from the Z_{Fe} determination). We also use the maximum MLDs associated with each location for the specific year. Uncertainty in each MLD determination is assessed using a climatology at ±2 standard deviation.

Diapycnal input is calculated by taking $\partial Fe/\partial z$ at the MLD (Supplementary Figure 2b) from Argo and multiplying by an estimate of vertical diffusivity (k_z, see main text). Winter entrainment is computed by integrating DFe down to the MLD_{MAX} from Argo. The proportion of the DFe stock entrained in the ML during winter that is detrained during springtime mixed-layer shallowing can be estimated using the MLD_{MAX}:MLD_{MIN} ratio from Argo at each DFe profile location (average = 3.16±1.86, see Supplementary Figure 2c for a representation of this term). Finally, the Ekman upwelling/downwelling of DFe requires the mean mixed layer DFe from DFe observations and Argo alongside the wind stress curl. For windstress we used the Quick Scatterometer Mean Wind Field (QuickSCAT MWF) gridded product (this global half degree-resolution product is processed and distributed by the Centre European Remote Sensing Satellite (ERS) d'Archivage et de Traitement (CERSAT); available online at http://www.ifremer.fr/cersat/). We used weekly maps of wind stress between 1999 and 2009 to produce monthly mean maps over a period consistent with the Argo data. The stated error of the product is less than $7x10^{-3}$ Pa over the area studied.

To estimate Z_{FeMAX}, we used the robust relationship between Z_{Fe} and density (Figure 1b) and since Z_{Fe} is below the diabatic surface layer for most profiles we determined Z_{FeMAX} by assuming that Z_{Fe} conserves its density. Thus the change in the density profile between the time of measurement and the time of MLD_{MAX} drives the 'winter' DFe profile. The resulting profiles are illustrated for four

313 case study regions in Supplementary Figure 4.

314

315 The iron utilisation estimates combine regionally optimised NPP determinations from ocean
316 colour[36] with combination with estimates of the biogeography in algal Fe/C ratios to arrive at
317 annual Fe utilisation estimates (1996 to 2007). The algal Fe/C ratios are applied using laboratory
318 data from Southern Ocean isolates[7,49]. For reference, the median annual Fe utilisation map from
319 ref(7) is reproduced in Supplementary Figure 5a.

320

321 **References**

322 1 Boyd, P. W. & Ellwood, M. J. The biogeochemical cycle of iron in the ocean. *Nature*
323 *Geoscience* **3**, 675-682, doi:10.1038/ngeo964 (2010).

324 2 Moore, C. M. *et al.* Processes and patterns of oceanic nutrient limitation. *Nature*
325 *Geoscience*, doi:10.1038/ngeo1765 (2013).

326 3 Sarmiento, J. L., Hughes, T. M. C., Stouffer, R. J. & Manabe, S. Simulated response of the
327 ocean carbon cycle to anthropogenic climate warming. *Nature* **393**, 245-249,
328 doi:10.1038/30455 (1998).

329 4 Takahashi, T. *et al.* Climatological mean and decadal change in surface ocean pCO2, and
330 net sea–air CO2 flux over the global oceans. *Deep Sea Research Part II: Topical Studies in*
331 *Oceanography* **56**, 554-577, doi:10.1016/j.dsr2.2008.12.009 (2009).

332 5 Boyd, P. W. *et al.* Climate-mediated changes to mixed-layer properties in the Southern
333 Ocean: assessing the phytoplankton response. *Biogeosciences* **5**, 847-864 (2008).

334 6 Tagliabue, A. *et al.* A global compilation of dissolved iron measurements: focus on
335 distributions and processes in the Southern Ocean. *Biogeosciences* **9**, 2333-2349,
336 doi:10.5194/bg-9-2333-2012 (2012).

337 7 Boyd, P. W., Arrigo, K. R., Strzepek, R. & van Dijken, G. L. Mapping phytoplankton iron
338 utilization: Insights into Southern Ocean supply mechanisms. *Journal of Geophysical*
339 *Research* **117**, doi:10.1029/2011jc007726 (2012).

8 Tagliabue, A. *et al.* Hydrothermal contribution to the oceanic dissolved iron inventory. *Nature Geoscience* **3**, 252-256, doi:10.1038/ngeo818 (2010).

9 Boyd, P. W., Ibisanmi, E., Sander, S. G., Hunter, K. A. & Jackson, G. A. Remineralization of upper ocean particles: Implications for iron biogeochemistry. *Limnology and Oceanography* **55**, 1271-1288, doi:10.4319/lo.2010.55.3.1271 (2010).

10 Moore, J. K., Doney, S. C., Glover, D. M. & Fung, I. Y. Iron cycling and nutrient-limitation patterns in surface waters of the World Ocean. *Deep-Sea Res Pt Ii* **49**, 463-507 (2002).

11 Watson, A. J. in *The biogeochemical cycle of iron in seawater* (ed Keith David R. Turner, A. Hunter) Ch. 2, (John Wiley and Sons, 2001).

12 Debaar, H. J. W. *et al.* Importance of Iron for Plankton Blooms and Carbon-Dioxide Drawdown in the Southern-Ocean. *Nature* **373**, 412-415, doi:Doi 10.1038/373412a0 (1995).

13 Toggweiler, J. R. & Russell, J. Ocean circulation in a warming climate. *Nature* **451**, 286-288, doi:10.1038/nature06590 (2008).

14 Boyd, P. W. *et al.* Microbial control of diatom bloom dynamics in the open ocean. *Geophysical Research Letters* **39**, doi:10.1029/2012gl053448 (2012).

15 Frew, R. D. *et al.* Particulate iron dynamics during FeCycle in subantarctic waters southeast of New Zealand. *Global Biogeochemical Cycles* **20**, doi:10.1029/2005gb002558 (2006).

16 Bowie, A. R. *et al.* Biogeochemical iron budgets of the Southern Ocean south of Australia: Decoupling of iron and nutrient cycles in the subantarctic zone by the summertime supply. *Global Biogeochemical Cycles* **23**, doi:10.1029/2009gb003500 (2009).

17 Boyd, P. W. *et al.* FeCycle: Attempting an iron biogeochemical budget from a mesoscale SF6 tracer experiment in unperturbed low iron waters. *Global Biogeochemical Cycles* **19**, doi:10.1029/2005gb002494 (2005).

18 Croot, P. L. *et al.* Physical mixing effects on iron biogeochemical cycling: FeCycle experiment. *Journal of Geophysical Research* **112**, doi:10.1029/2006jc003748 (2007).

19 Johnson, K. S., Gordon, R. M. & Coale, K. H. What controls dissolved iron concentrations

in the world ocean? *Marine Chemistry* **57**, 137-161, doi:10.1016/s0304-4203(97)00043-1 (1997).

20 Sallée, J.-B., Speer, K., Rintoul, S. & Wijffels, S. Southern Ocean Thermocline Ventilation. *Journal of Physical Oceanography* **40**, 509-529, doi:10.1175/2009jpo4291.1 (2010).

21 Law, C. S. Vertical eddy diffusion and nutrient supply to the surface mixed layer of the Antarctic Circumpolar Current. *Journal of Geophysical Research* **108**, doi:10.1029/2002jc001604 (2003).

22 Cisewski, B., Strass, V. H. & Prandke, H. Upper-ocean vertical mixing in the Antarctic Polar Front Zone. *Deep-Sea Res Pt Ii* **52**, 1087-1108, doi:10.1016/J.Dsr2.2005.01.010 (2005).

23 Wu, L., Jing, Z., Riser, S. & Visbeck, M. Seasonal and spatial variations of Southern Ocean diapycnal mixing from Argo profiling floats. *Nature Geoscience* **4**, 363-366, doi:10.1038/ngeo1156 (2011).

24 Frants, M. *et al.* Analysis of horizontal and vertical processes contributing to natural iron supply in the mixed layer in southern Drake Passage. *Deep Sea Research Part II: Topical Studies in Oceanography* **90**, 68-76, doi:10.1016/j.dsr2.2012.06.001 (2013).

25 Ellwood, M. J., Boyd, P. W. & Sutton, P. Winter-time dissolved iron and nutrient distributions in the Subantarctic Zone from 40–52S; 155–160E. *Geophysical Research Letters* **35**, doi:10.1029/2008gl033699 (2008).

26 Wagener, T., Guieu, C., Losno, R., Bonnet, S. & Mahowald, N. Revisiting atmospheric dust export to the Southern Hemisphere ocean: Biogeochemical implications. *Global Biogeochemical Cycles* **22**, doi:10.1029/2007gb002984 (2008).

27 Lannuzel, D. *et al.* Distribution of dissolved iron in Antarctic sea ice: Spatial, seasonal, and inter-annual variability. *Journal of Geophysical Research* **115**, doi:10.1029/2009jg001031 (2010).

28 Lin, H., Rauschenberg, S., Hexel, C. R., Shaw, T. J. & Twining, B. S. Free-drifting icebergs

as sources of iron to the Weddell Sea. *Deep Sea Research Part II: Topical Studies in Oceanography* **58**, 1392-1406, doi:10.1016/j.dsr2.2010.11.020 (2011).

29 Raiswell, R., Benning, L. G., Tranter, M. & Tulaczyk, S. Bioavailable iron in the Southern Ocean: the significance of the iceberg conveyor belt. *Geochemical transactions* **9**, 7, doi:10.1186/1467-4866-9-7 (2008).

30 Gerringa, L. J. A. *et al.* Iron from melting glaciers fuels the phytoplankton blooms in Amundsen Sea (Southern Ocean): Iron biogeochemistry. *Deep Sea Research Part II: Topical Studies in Oceanography* **71-76**, 16-31, doi:10.1016/j.dsr2.2012.03.007 (2012).

31 Nishioka, J., Ono, T., Saito, H., Sakaoka, K. & Yoshimura, T. Oceanic iron supply mechanisms which support the spring diatom bloom in the Oyashio region, western subarctic Pacific. *Journal of Geophysical Research* **116**, doi:10.1029/2010jc006321 (2011).

32 Sarthou, G. *et al.* The fate of biogenic iron during a phytoplankton bloom induced by natural fertilisation: Impact of copepod grazing. *Deep Sea Research Part II: Topical Studies in Oceanography* **55**, 734-751, doi:10.1016/j.dsr2.2007.12.033 (2008).

33 Strzepek, R. F. *et al.* Spinning the "Ferrous Wheel": The importance of the microbial community in an iron budget during the FeCycle experiment. *Global Biogeochemical Cycles* **19**, GB4S26, doi:10.1029/2005gb002490 (2005).

34 Sunda, W. G. & Huntsman, S. A. Iron uptake and growth limitation in oceanic and coastal phytoplankton. *Marine Chemistry* **50**, 189-206, doi:10.1016/0304-4203(95)00035-p (1995).

35 Marchetti, A. *et al.* Ferritin is used for iron storage in bloom-forming marine pennate diatoms. *Nature* **457**, 467-470, doi:10.1038/nature07539 (2009).

36 Arrigo, K. R., van Dijken, G. L. & Bushinsky, S. Primary production in the Southern Ocean, 1997–2006. *Journal of Geophysical Research* **113**, doi:10.1029/2007jc004551 (2008).

37 Mackie, D. S. *et al.* Biogeochemistry of iron in Australian dust: From eolian uplift to marine uptake. *Geochemistry, Geophysics, Geosystems* **9**, doi:10.1029/2007gc001813 (2008).

38 Gaiero, D. M., Probst, J. L., Depetris, P. J., Bidart, S. M. & Leleyter, L. Iron and other

transition metals in Patagonian riverborne and windborne materials: Geochemical control and transport to the southern South Atlantic Ocean. *Geochimica Et Cosmochimica Acta* **67**, 3603-3623, doi:Doi 10.1016/S0016-7037(03)00211-4 (2003).

39 Stammerjohn, S., Massom, R., Rind, D. & Martinson, D. Regions of rapid sea ice change: An inter-hemispheric seasonal comparison. *Geophysical Research Letters* **39**, n/a-n/a, doi:10.1029/2012gl050874 (2012).

40 Dierssen, H. M. Perspectives on empirical approaches for ocean color remote sensing of chlorophyll in a changing climate. *Proceedings of the National Academy of Sciences of the United States of America* **107**, 17073-17078, doi:10.1073/pnas.0913800107 (2010).

41 Lovenduski, N. S. & Gruber, N. Impact of the Southern Annular Mode on Southern Ocean circulation and biology. *Geophysical Research Letters* **32**, doi:10.1029/2005gl022727 (2005).

42 Séférian, R. *et al.* Skill assessment of three earth system models with common marine biogeochemistry. *Climate Dynamics* **40**, 2549-2573, doi:10.1007/s00382-012-1362-8 (2012).

43 Steinacher, M. *et al.* Projected 21st century decrease in marine productivity: a multi-model analysis. *Biogeosciences* **7**, 979-1005 (2010).

44 Misumi, K. *et al.* The iron budget in ocean surface waters in the 20th and 21st centuries: projections by the Community Earth System Model version 1. *Biogeosciences Discussions* **10**, 8505-8559, doi:10.5194/bgd-10-8505-2013 (2013).

45 Marinov, I., Doney, S. C. & Lima, I. D. Response of ocean phytoplankton community structure to climate change over the 21st century: partitioning the effects of nutrients, temperature and light. *Biogeosciences* **7**, 3941-3959, doi:10.5194/bg-7-3941-2010 (2010).

46 Henson, S., Cole, H., Beaulieu, C. & Yool, A. The impact of global warming on seasonality of ocean primary production. *Biogeosciences* **10**, 4357-4369, doi:10.5194/bg-10-4357-2013 (2013).

444 47 Sallee, J. B., Wienders, N., Speer, K. & Morrow, R. Formation of subantarctic mode water
445 in the southeastern Indian Ocean. *Ocean Dynamics* **56**, 525-542, doi:Doi 10.1007/S10236-
446 005-0054-X (2006).
447 48 de Boyer Montegut, C., Madec, G., Fischer, A. S., Lazar, A. & Iudicone, D. Mixed layer
448 depth over the global ocean: An examination of profile data and a profile-based climatology.
449 *J Geophys Res-Oceans* **109**, doi:10.1029/2004jc002378 (2004).
450 49 Strzepek, R. F., Maldonado, M. T., Hunter, K. A., Frew, R. D. & Boyd, P. W. Adaptive
451 strategies by Southern Ocean phytoplankton to lessen iron limitation: Uptake of organically
452 complexed iron and reduced cellular iron requirements. *Limnology and Oceanography* **56**,
453 1983-2002, doi:10.4319/lo.2011.56.6.1983 (2011).
454

455 **Acknowledgements**

456 We thank all observational scientists that generously shared dissolved iron data (especially M.
457 Klunder and P. Sedwick who did so before publication), the GEOTRACES programme
458 (www.geotraces.org), Kevin Arrigo and Gert van Dijken for providing iron utilisation data files and
459 Andrew Barton for comments on the manuscript. The Argo float data were collected and made
460 freely available by the International Argo Program (http://www.argo.ucsd.edu). This work
461 benefitted from the support of the French Agence Nationale de la Recherche (ANR) grant ANR-10-
462 LABX-18-01 of the national Programme Investissements d'Avenir, the CSIR Parliamentary Grant,
463 NRF-SANAP and the EU FP7 Marie Curie International Research Staff Exchange Scheme (IRSES)
464 Fellowship SOCCLI (The role of Southern Ocean Carbon cycle under CLImate change), which
465 received funding from the European Commission's Seventh Framework Programme under grant
466 agreement 317699. JBS received support from Agence Nationale de la Recherche (ANR), ANR-12-
467 PDOC-0001, as well as from the British Antarctic Survey as a BAS Fellow. This research was
468 partly supported by the Australian Government Cooperative Research Centres Programme through
469 the Antarctic Climate and Ecosystems CRC (ACE CRC), University of Tasmania Rising Stars grant

#B0019024 and Australian Antarctic Science project #2900, the New Zealand Ministry for Science and Innovation and the Institute of Marine and Antarctic Studies, University of Tasmania. The final manuscript was improved thanks to the comments of two anonymous reviewers.

Author Contributions

Led design of the study and writing of the manuscript (A.T), assembly of the iron and Argo datasets and data analysis (A.T and J-B.S), additional physical flux analyses (A.T., J-B.S, M.L and S.S), biological rate measurements (P.W.B) and additional iron observations (A.R.B). All authors contributed to the overall experimental work, discussion of the results and their implications, as well as commenting on the manuscript.

Figure Legends:

Figure 1. Depths and potential density of the ferricline and its seasonal evolution. a) The depth of the ferricline (m, black and grey triangles denote the mean and median, respectively), b) the potential density anomaly (σ_θ, kg m^{-3}) associated with the ferricline depth and c) box and whisker plots of the seasonal cycle in MLD, Z_{Fe} and Z_{Fe}-MLD (the size of the box represents the 1st to 3rd quartiles, with the vertical bar corresponding to the median and the whiskers representing 1.5 times the inter-quartile range). While calculations for panels a and b are performed on a 1° grid, they are shown using a 3° grid for clarity, the 3000m isobath and the mean Polar Front position (black line[6]) are also displayed.

Figure 2. The relationship between the ferricline and mixed layer depths and calculations of physically-mediated iron fluxes. a) A histogram of the offset (m) between the depth of the ferricline and the mixed layer depth (blue and red for concomitant and winter MLDs, respectively), b) annual diapycnal diffusion flux of Fe across the mixed-layer (mmol m^{-2} yr^{-1}), c) annual entrainment flux of Fe (mmol m^{-2} yr^{-1}) and d) annual Ekman DFe term (mmol m^{-2} yr^{-1}), with a negative/positive values indicating downwelling/upwelling of DFe. In panels b-d black and grey triangles denote the mean and median, respectively. Gridding for panels b-d as for Figure 1a.

Figure 3. Assessments of how different physically-mediated iron supply mechanisms compare to utilisation and their contribution to total iron fluxes. The percentage of locations where a) diapycnal diffusion and b) entrainment can match iron utilisation over different scenarios regarding the *f*e-ratio and k_z (panel a) and detrainment (panel b). The proportional contribution of c) diapycnal diffusion and d) entrainment to total physical DFe supply (see supplementary Figure 3b). Gridding for panels c and d as for Figure 1a.

Figure 4. A schematic representation of the seasonal variability in Southern Ocean Fe cycling. We emphasise seasonal changes in the physical supply of Fe (blue arrows), mixed layer depth and the mixed layer DFe inventory, as well as the magnitude of recycling (orange-red arrows) and pelagic community composition. The dominant physical processes over the season is conceptualised at the bottom of the figure. We note that some recycling likely occurs below the mixed-layer and can be entrained the following winter.

a) Ferricline Depth (m)

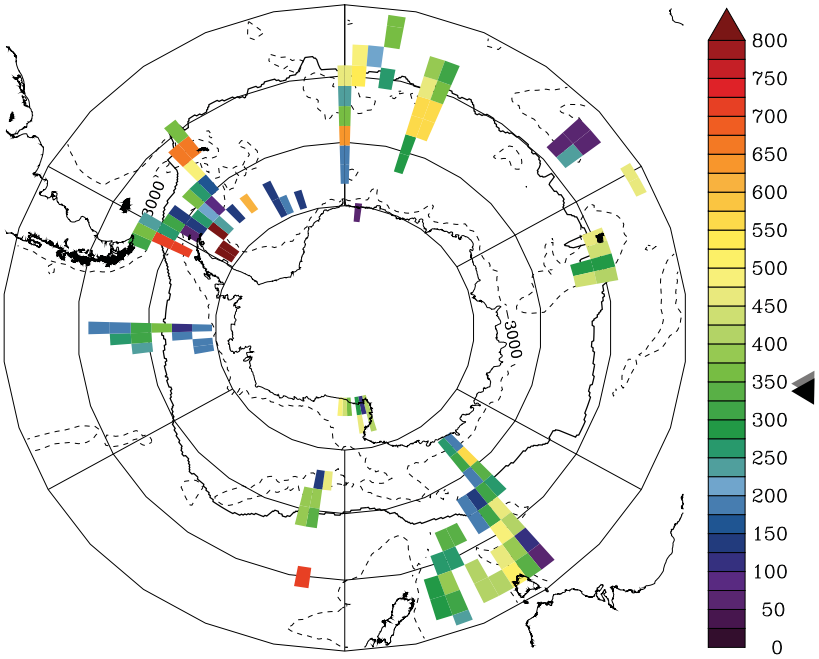

b) σ_0 at the Ferricline depth (kg m^{-3})

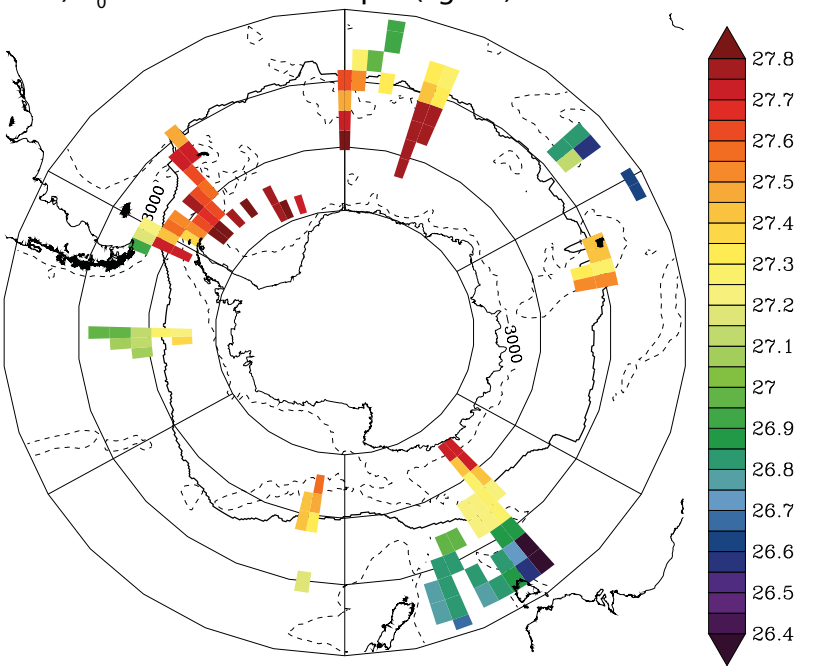

c) Ferricline, Mixed Layer Depths and Offset

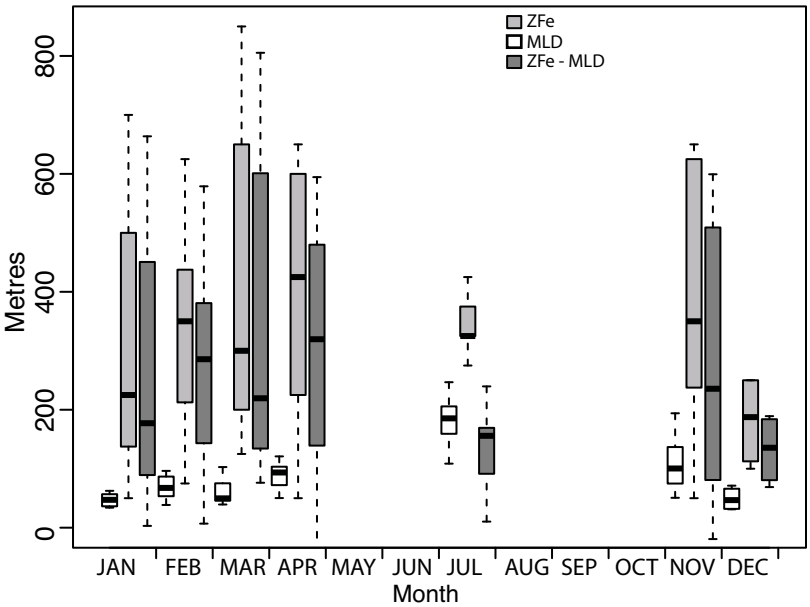

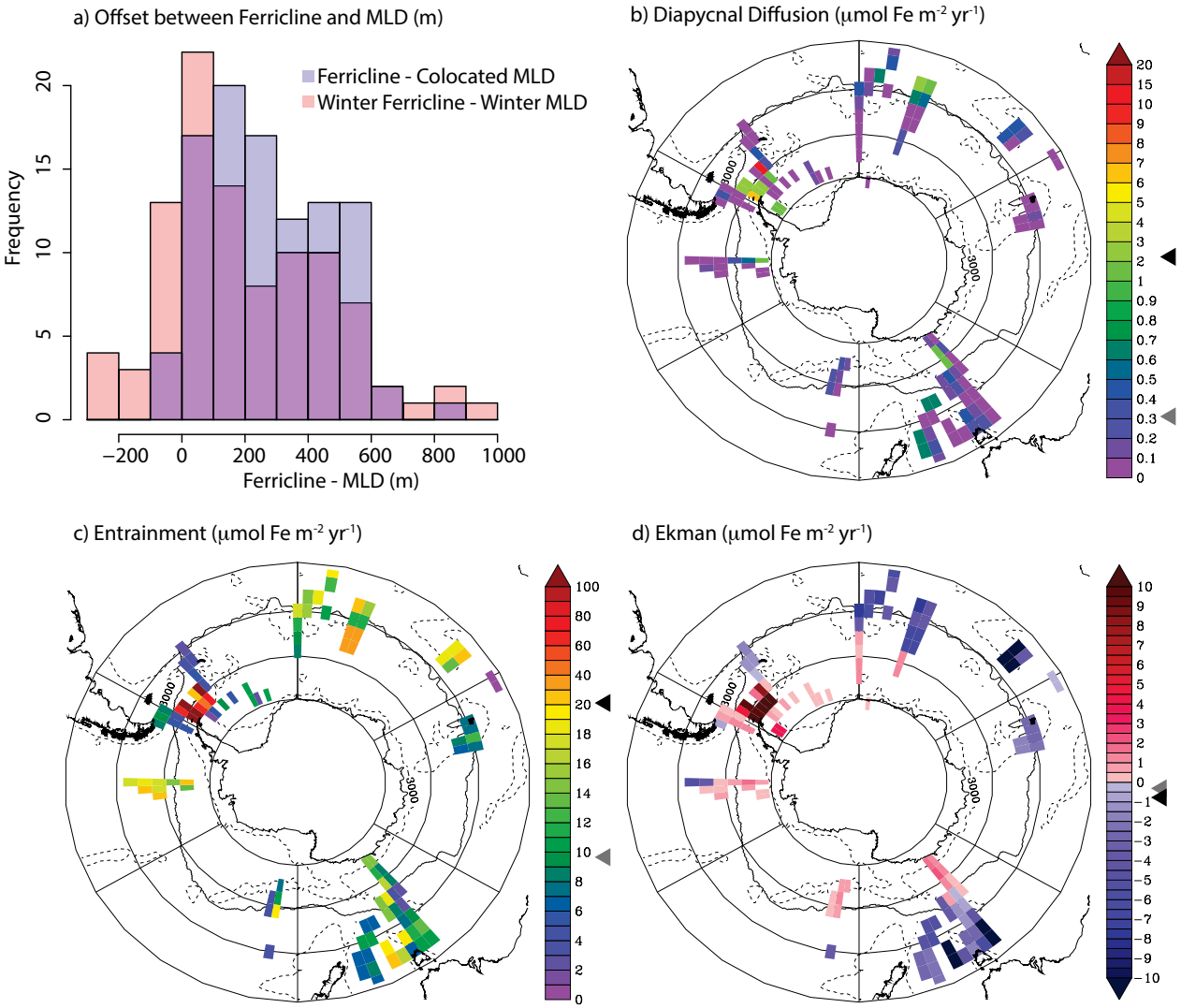
a) Offset between Ferricline and MLD (m)
Ferricline - Colocated MLD
Winter Ferricline - Winter MLD
Frequency
0
5
10
15
20
−200
0
200
400
600
800
1000
Ferricline - MLD (m)
b) Diapycnal Diffusion (μmol Fe m-2 yr-1)
20
15
10
9
8
7
6
5
4
3
2
1
0.9
0.8
0.7
0.6
0.5
0.4
0.3
0.2
0.1
0
3000
c) Entrainment (μmol Fe m-2 yr-1)
100
80
60
40
20
18
16
14
12
10
8
6
4
2
0
d) Ekman (μmol Fe m-2 yr-1)
10
9
8
7
6
5
4
3
2
1
0
−1
−2
−3
−4
−5
−6
−7
−8
−9
−10

a) Percent of Locations where Diapycnal Diffusion Matches Iron Utilisation

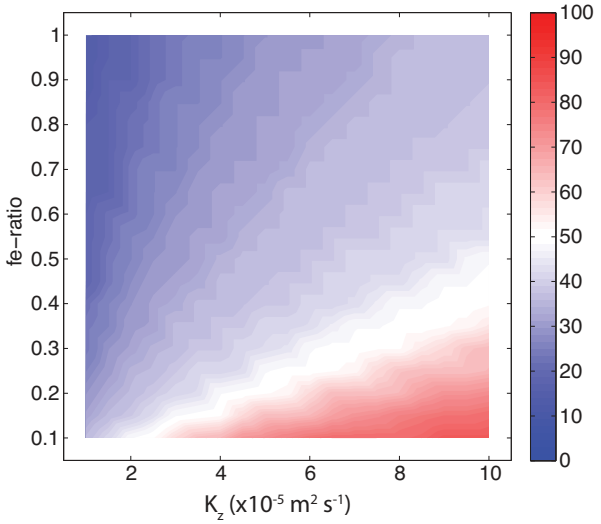

b) Percent of Locations where Entrainment Matches Iron Utilisation

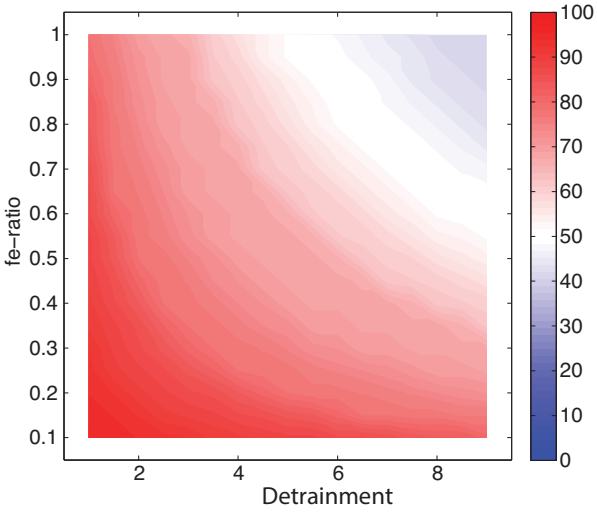

c) Relative Importance of Diapycnal Diffusion

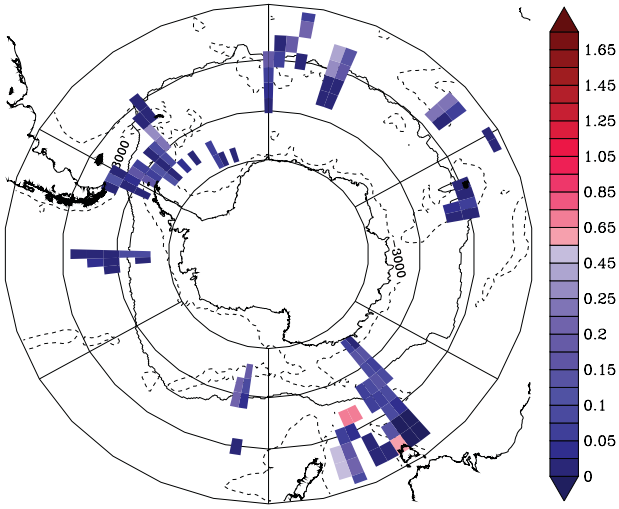

d) Relative Importance of Entraiment

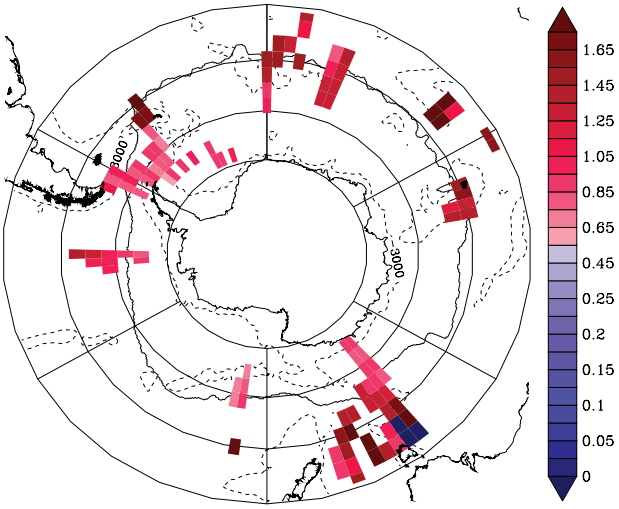

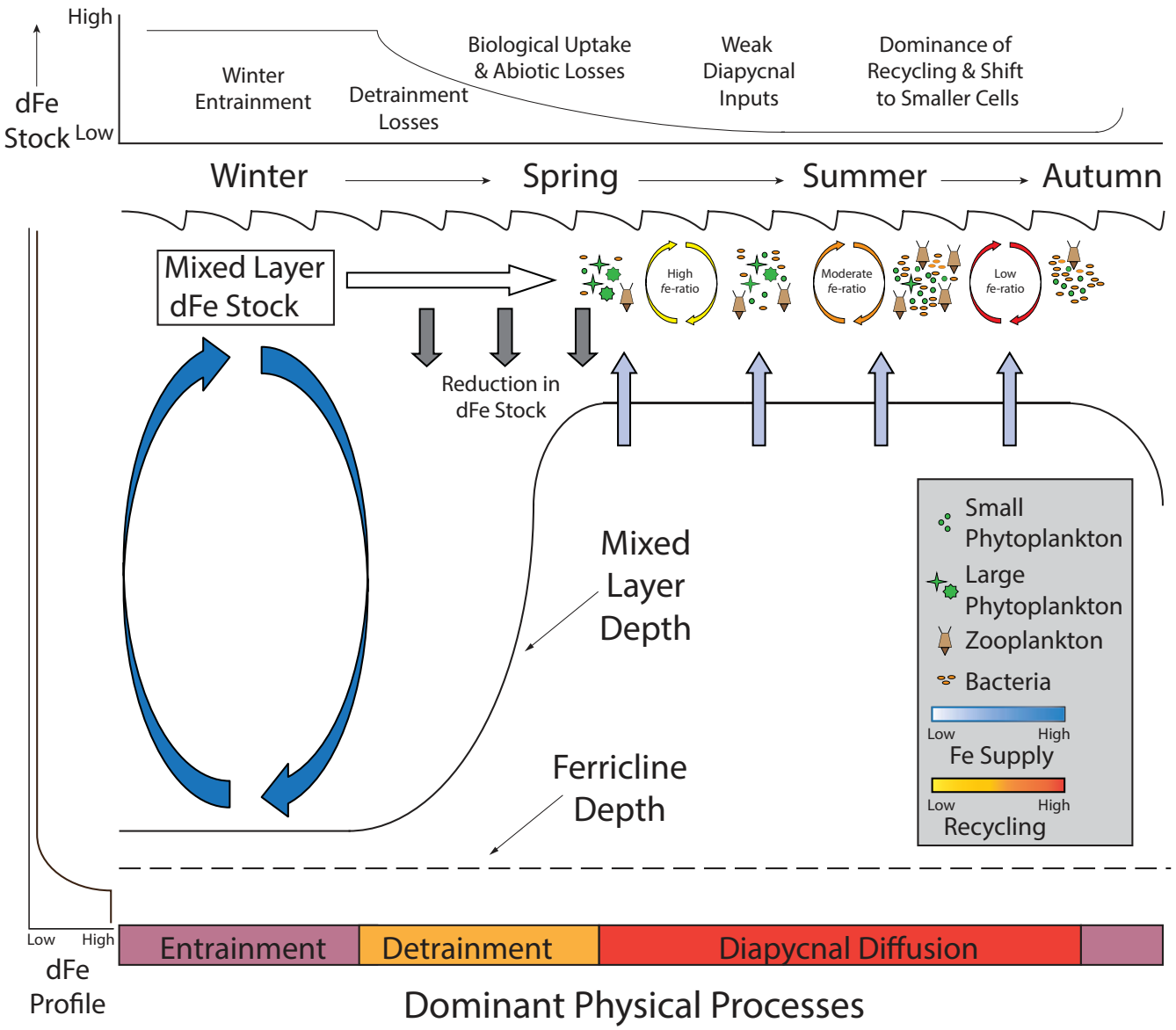
High
dFe
Stock
Low
Winter
Entrainment
Detrainment
Losses
Biological Uptake
& Abiotic Losses
Weak
Diapycnal
Inputs
Dominance of
Recycling & Shift
to Smaller Cells
Winter
Spring
Summer
Autumn
Mixed Layer
dFe Stock
High
fe-ratio
Moderate
fe-ratio
Low
fe-ratio
Reduction in
dFe Stock
Mixed
Layer
Depth
Small
Phytoplankton
Large
Phytoplankton
Zooplankton
Bacteria
Low
High
Fe Supply
Low
High
Recycling
Ferricline
Depth
Low
High
dFe
Profile
Entrainment
Detrainment
Diapycnal Diffusion
Dominant Physical Processes